Research Article Vol. 3, No. 10 / 15 October 2020 / OSA Continuum 2741

Compact picosecond mid-IR PPLN OPO with controllable peak powers

YUDI WU, SIJING LIANG, QIANG FU, LIN XU,* AND DAVID J. RICHARDSON

Optoelectronics Research Centre, University of Southampton, Southampton, SO17 1BJ, UK
**l.xu@soton.ac.uk*

Abstract: We report a high-repetition-rate, compact, mid-infrared picosecond (ps) optical parametric oscillator (OPO) based on periodically poled lithium niobate (PPLN). The OPO is synchronously pumped by an ytterbium-doped-fibre (YDF) master-oscillator-power-amplifier (MOPA) system, seeded by a 1040-nm gain-switched laser diode (GSLD). Under continuous-wave (cw) pulsed operation, at a 1.5-GHz repetition rate and 14-W pump power, an idler average power of 2.4 W (~30 W peak power) was achieved, with an idler wavelength tunability of 2260–3573 nm. Through the addition of an electro-optic modulator (EOM) to the MOPA system, acting as a time gate to suppress a variable number of pulses per 1 μs, a quasi-cw pumping regime was realized, allowing burst-mode operation of the OPO at a 1-MHz inter-burst repetition rate. By varying the burst window time with the EOM, controllable idler peak powers of up to 1.2 kW were then realized.

1. Introduction

Ultrashort-pulsed mid-infrared (MIR) lasers have many important applications such as spectroscopy, material processing and free-space communications [1–3]. In these applications, features including processing speed and signal-to-noise ratio are significantly enhanced by pulse parameters such as a high repetition rate and high peak power [4,5]. Optical parametric oscillators (OPOs) are commonly used as MIR laser sources through frequency conversion from the near infrared. However, OPOs require temporal synchronization between the pump and the resonated signal when used to produce ultrashort pulses. Hence, conventional picosecond (ps) OPO systems normally operate with a short cavity length for high-repetition-rate pulses with low peak power [6], or with a relatively long cavity length for pulses at low repetition rate and high peak power [7]. Other techniques such as high-harmonic-cavity OPO and intra-cavity-pumped OPO could reduce the OPO cavity length for low repetition rate, however, those solutions either require high intense pump pulse or complex cavities [8,9]. Compared to these techniques, burst-mode OPOs, pumped by a burst of pulses with a high intra-burst pulse repetition rate but a low inter-burst pulse repetition rate, allows a short cavity length while simultaneously achieve high peak power and high repetition rate [10–12]. Such burst pulsed lasers offer enhanced imaging quality in photoacoustic spectroscopy [13], improved thermal management in tissue ablation process [14] and enabled laser-jamming of heat sinking missiles [15]. Intra-burst pulse repetition rate of 48-MHz mode-locked laser pumped OPO has been demonstrated in [12] and an OPO with a higher intra-burst pulse repetition rate of 1.1 GHz was reported in [10]. However, an external pulse multiplier was employed to increase the pump laser fundamental repetition rate, which caused uneven intra-burst pulse amplitude so that affected the generated MIR pulse energy uniformity and associated pump-to-idler conversion efficiency. Here we report a high-repetition-rate MIR OPO pumped using a gain-switched laser-diode (GSLD) seeded 1-μm fibre-laser system that provides both continuous-wave (cw) pulsed and burst-pulse operation. The GSLD provides

#400213 https://doi.org/10.1364/OSAC.400213
Journal © 2020 Received 15 Jun 2020; revised 3 Sep 2020; accepted 3 Sep 2020; published 22 Sep 2020

OSA CONTINUUM

uniform pulse train with 1.5-GHz repetition rate that allows a synchronously-pumped OPO with compact cavity and high conversion efficiency. Generally, in burst-mode OPOs, resonated signals build up from spontaneous noise to steady oscillation repeatedly over each burst window, and therefore the burst-window duration and individual pulse peak powers are important parameters that affect the OPO operation and efficiency. Studies of these parameters are thus needed to understand the dynamics of the pulse evolution process and guide the design of the burst-mode OPO. In our fibre-laser system, a burst-pulse picker with adjustable time window provides a good flexibility to control the burst-window duration and the individual pulse peak powers. The OPO consists of a periodically poled lithium niobate (PPLN) nonlinear gain medium to generate tunable idler wavelengths from 2260 nm to 3573 nm. In cw-pulsed operation, the OPO generates idler average power of 2.4 W and a maximum power conversion efficiency of 23%. In burst-mode operation, the OPO performance is studied with respect to the burst-window duration and the oscillation build-up time. Stable OPO operation has been successfully demonstrated by pumping with a minimum number of 30 intra-burst pulses. The burst-mode OPO offers MIR idler pulses with controllable peak power from 30 W up to 1.2 kW.

2. Experimental setup

The OPO pump source is an ytterbium-doped-fibre (YDF) master-oscillator-power-amplifier (MOPA) system, seeded by a 1040-nm GSLD. The schematic setup of the MOPA system is illustrated in Fig. 1 (excluding the red box). The GSLD (1064CHP, 3SPhotonics) seed laser was operated at a 1.5-GHz repetition rate, producing 37-ps pulses at 1040 nm with a 1-mW average output power. The MOPA consisted of three YDF amplifier stages including a core-pumped polarization-maintaining (PM) YDF (PM-YDF-5/130-VIII, Nufern) with a 5-μm core diameter as the first stage, a cladding-pumped PM YDF (PMLA-YDF-10/125-VIII, Nufern) with an 11-μm core and 125-μm cladding diameter as the second stage, and a cladding-pumped PM YDF (PMLA-YDF-25/250-VIII, Nufern) with a 25-μm core and 250-μm cladding diameter as the third stage. The pump laser diodes (LDs) for the MOPA amplification stages were a 980-nm single-mode LD with 200-mW launch power in the first stage, 976-nm multi-mode LD with 1.5-W launch power in the second stage and 975-nm wavelength-stabilized multi-mode LD with 20-W launch power in the third stage, respectively. The core pumped YDF used in the first stage amplifier had a length of 80 cm, and the lengths of cladding pumped YDF used in the second and third stage amplifiers was 3 m and 3.5 m respectively. The MOPA provided an average output power of up to 14 W. The output optical spectrum at maximum power is centered around 1040 nm with a 3-dB bandwidth of 0.1 nm, as shown in Fig. 2(a). Note that the floor of the pump spectrum [Fig. 2(a)] appears asymmetric which is due to the amplified spontaneous emission spectral level being asymmetric with a peak located at a longer wavelength than the 1040 nm signal wavelength. The MOPA output pulse was measured using the combination of a 32-GHz-bandwidth photo-detector (83440D, Agilent) and a 20-GHz-bandwidth digital communication analyzer (Infiniium 86100C, Agilent), providing a combined measurement bandwidth of ~17 GHz and rise time of ~20 ps. The pulse, presented in Fig. 2(b), was observed to have a slightly increased duration of 40 ps. To control the polarization of the OPO pump, a half-wave plate was placed at the MOPA output (HWP in Fig. 3).

To achieve burst-mode operation, an electro-optic modulator (EOM) and an extra core-pumped fibre-amplification stage (the red box in Fig. 1) was inserted between the first and second YDF amplifier stages such that the EOM could be employed as a time gate to suppress a variable number of pulses every 1 μs, with a 1-MHz inter-burst repetition rate [Fig. 2(c)]. Due to the gain-saturated operation of the final-stage amplifier, in burst-mode operation, in spite of the variable burst-window durations, the maximum output power of the MOPA was constant at 14 W (with the same pump power).

OSA CONTINUUM

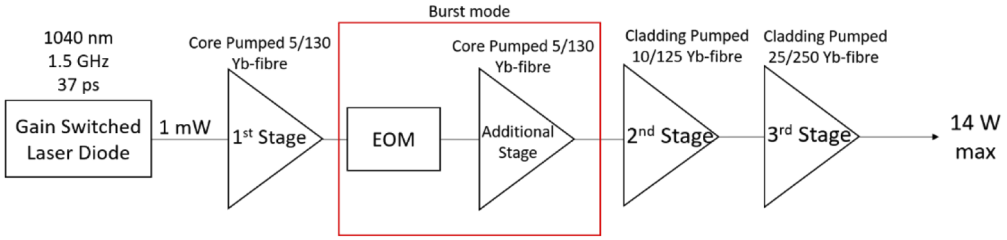

Fig. 1. Schematics of the MOPA pump. In burst mode operation, an EOM and an extra YDF amplifier stage were inserted into the MOPA (red box).

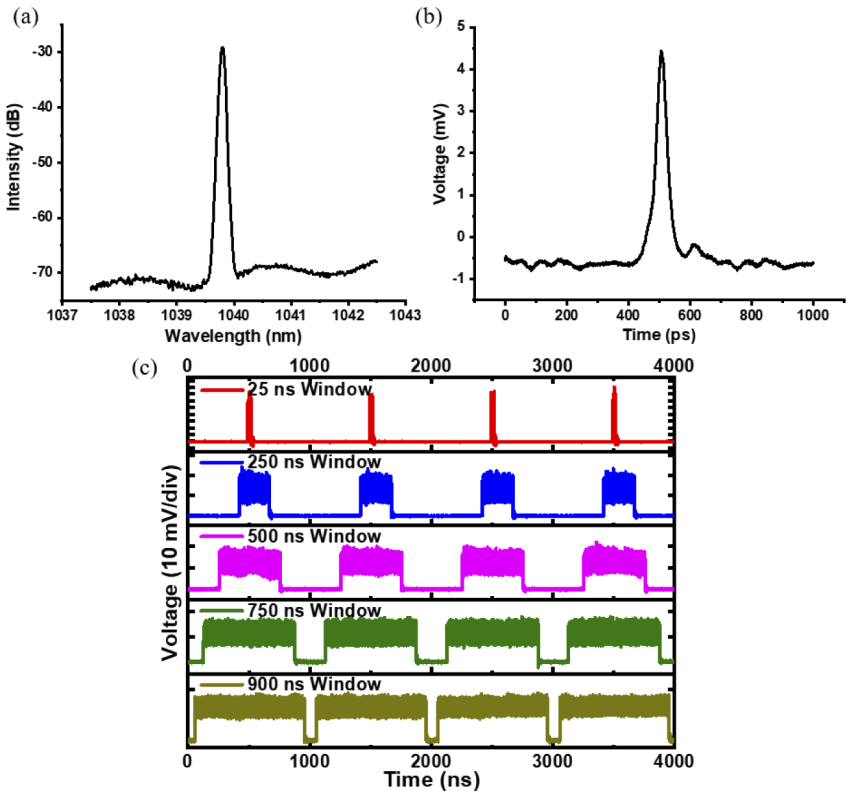

Fig. 2. Graphs showing MOPA's (a) optical spectrum, (b) temporal pulse shape and (c) pulse trace under burst mode operation (note the different vertical scales in (c)).

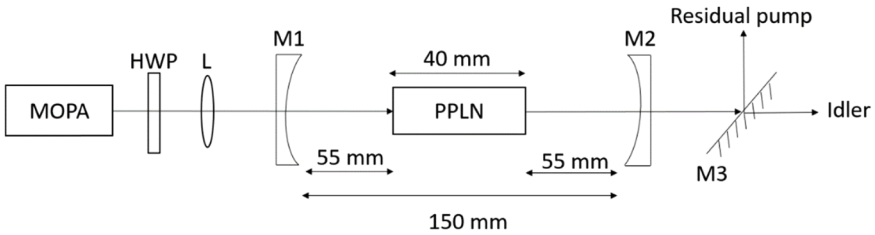

Fig. 3. Schematics of the OPO. HWP: half-wave plate; L: lens; M1, M2: concave mirrors; M3; 45° dichroic mirror.

OSA CONTINUUM

The OPO was of a signal-resonant linear-cavity design, consisting of two concave mirrors with a 40-mm-long PPLN nonlinear crystal. A schematic of the OPO cavity is presented in Fig. 3. Both mirrors (M1 and M2 in Fig. 3) had a radius of curvature of 100 mm and were of high reflectivity (>99%) at wavelengths around 1.5 μm (signal) and ~81% transmission at around both 1 μm (pump) and 3 μm (idler). A compact linear-cavity with physical length of 15 cm was built to provide a half-harmonic synchronization to the 1.5-GHz intra-burst pulse repetition rate of the pump (i.e. two signal pulses circulating in the cavity), as well as to allow a small intra-cavity signal beam waist. A standard synchronous cavity was not used due to a mixture of lack of mirrors with shorter radius of curvature and also the physical difficulties in setting up the cavity with such short total free space length of ~1 cm. To match the signal cavity mode, which had a calculated beam radius of 87 μm, the MOPA output beam was focused down to a measured beam radius of 85 μm with a plano-convex lens of 150-mm focal length (L in Fig. 3). The 40-mm-long PPLN crystal (MOPO1-1.0-10, Covesion), had 5 poled gratings with periods ranging from 29.52–31.59 μm in steps of 0.5 μm. It was mounted in an oven that allowed temperature tuning from 20 to 200 °C. For the idler measurements, a 45° dichroic mirror (M3 in Fig. 3) of high reflectivity at 1 μm and 68.8% transmission at 3 μm, was placed after the OPO cavity to filter out the residual pump light.

3. Results and discussions

3.1. Continuous-wave pulsed operation

Under cw-pulsed operation, 2991.5-nm idler output was observed from the OPO with a pump average power threshold of 1.78 W. The output average power of the idler with respect to different pump powers is shown in Fig. 4, taking into account the transmissions of M2 and M3. In theory the full idler power could be accessible if M2 and M3 had an idler transmission nearer to 100%. The idler power increased linearly with respect to the pump power at a slope efficiency of 21.0%, reaching a maximum value of 2.4 W. The corresponding power conversion efficiency was achieved with a maximum value of 23% at 3-W pump power, where the quantum photon efficiency (idler photons output divided by pump photons input) reached 66.2%. At higher pump powers, though still above 20%, a decrease in conversion efficiency was observed (Fig. 4), which was likely due to back conversion at such high pump powers [16]. Thanks to the compact and stable optical cavity, the OPO output power had a good stability with only small fluctuations (<5%) that could be imposed by the combination of pump power variation and mechanical perturbation of the optics, however, no power drift was observed over a timescale of the order of an hour.

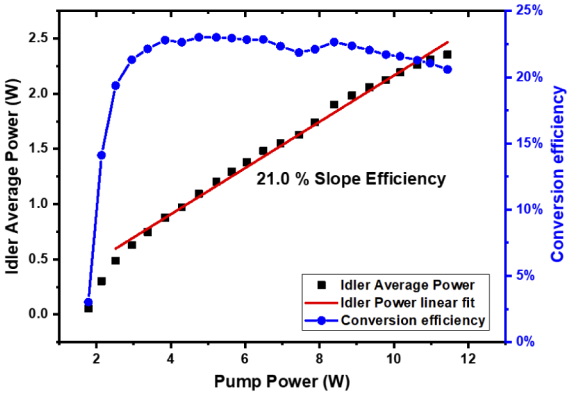

Fig. 4. Graph showing the OPO's average idler power (black) with linear fit (red) and conversion efficiency (blue dots) against pump power. The blue line is a guide for the eye.

OSA CONTINUUM

To characterize the idler wavelength tunability of the OPO, different PPLN grating periods and oven temperatures were used, and the output spectra were measured with an optical spectrum analyzer (721 series, Bristol instruments, 6-GHz resolution). A seamless wavelength tuning of the idler output across 2260–3573 nm was achieved and several spectra of different central wavelengths are shown in Fig. 5(a). The idler spectrum with a 2260-nm central wavelength shows a higher noise level due to the corresponding signal wavelength being very close to the edge of the high-reflectivity band of the cavity mirrors. A typical idler spectrum at 2991.5 nm had a full-width-at-half-maximum (FWHM) bandwidth of 0.65 nm, as shown in Fig. 5(b).

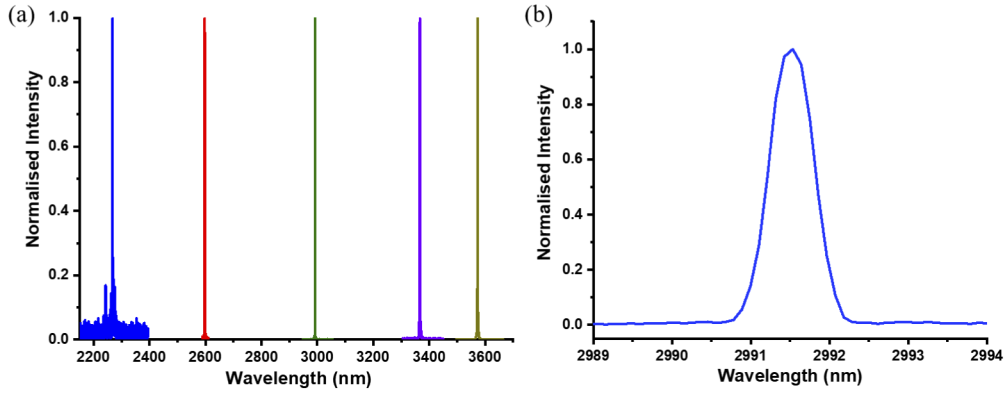

Fig. 5. Graphs showing (a) the tunability of the idler from the OPO and (b) a typical idler optical spectrum.

The idler beam quality was measured using a pyroelectric scanning profiler for different pump powers, including within the unsaturated and saturated OPO conversion efficiency region. A good beam quality with M_x^2 of 1.14 and M_y^2 of 1.09 was obtained at a pump power of 3 W, however, the beam quality was found to be degraded at higher pump power, reaching values of M_x^2 of 1.26 and M_y^2 of 1.10 at the maximum power, as shown in Fig. 6. It is believed that back-conversion and thermal effects in the OPO could be responsible for the lower output beam quality in this case [17]. The beam quality appears to degrade more in the horizontal x direction at maximum pump power making the beam elliptical at focus. This is likely due to angled endcap at the output of the final amplifier stage of the MOPA which causes pump beam to become elliptical and which can then excite higher order modes in the OPO cavity at high pump powers.

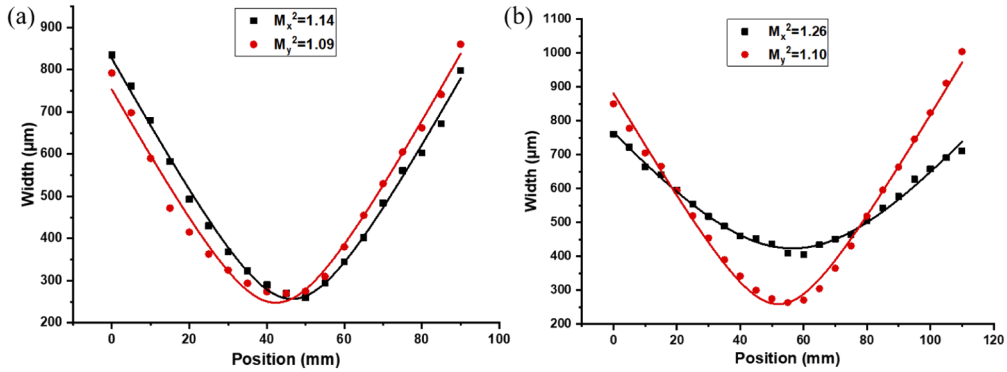

Fig. 6. Beam quality measurements at (a) low pump power and (b) at maximum pump power.

OSA CONTINUUM

3.2. Burst-mode operation

3.2.1. Peak power control

Bursts of 1.5-GHz-repetition-rate pulses, with constant average power but different numbers of pulses in each burst, were generated for pumping the OPO by varying the burst-pulse window with the EOM. The average power of the idler output was measured to vary from 1.4 to 2.4 W (Fig. 7) with the burst-pulse window set from 20 ns to 980 ns. The corresponding peak power of each individual idler pulse was then calculated and Fig. 7 shows the pulse peak power against the number of pulses for each burst mode. As the number of pulses per burst decreases, the idler pulse peak power increases significantly. Parametric oscillation was observed for a number of pulses per burst as low as 30, where an idler pulse peak power of 1.2 kW was achieved at a calculated parametric gain of 50 dB. This is two orders of magnitude higher than the idler pulse peak power of ~30 W achieved when the OPO was operating with a cw 1.5-GHz train of pulses. Thus, by using burst-mode operation, a highly compact MIR OPO with simultaneously high intra-burst repetition rate and high peak power was achieved.

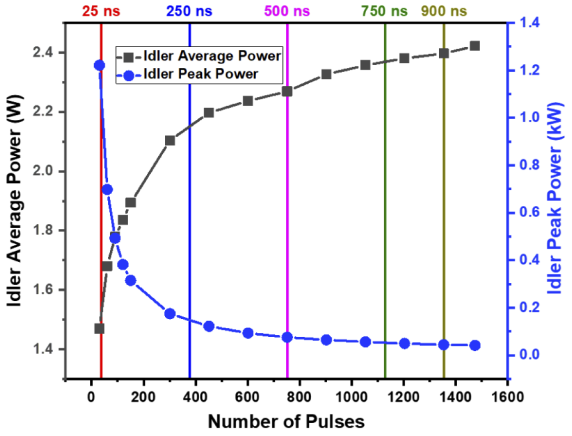

Fig. 7. Measurements of the OPO's idler average power and idler peak power. The vertical colored line marks the corresponding window time.

3.2.2. Study of cavity build-up

At constant average power, a smaller burst-pulse window provided a higher pump peak power in each individual pulse. Apart from controlling peak pulse power, burst-mode OPOs have also been shown to allow an increase in conversion efficiency compared to standard long-pulse OPOs of the same pump peak power [18] due to a reduction in the signal build-up time similar to that found using rectangular-shaped pump pulses [19]. However, it is interesting to note that we observed a decrease in idler average power and hence a decrease in conversion efficiency from our burst-mode OPO, as can be seen from the black data points in Fig. 7. This is because the ratio of the time required for cavity build-up to the overall burst-pulse time-window increases for smaller windows. However, the decrease in idler power is not linear with respect to the ratio between the burst-window duration and the burst period due to the fact that the pump peak pulse power is higher for a shorter burst window than for a longer burst window at the same average pump power. The measured pulse traces for the residual pump with 500-ns and 25-ns burst-pulse time-windows are presented in Fig. 8(a) and Fig. 8(b) respectively. It shows that pump is depleted rapidly at the start of the time-window before reaching a stabilized level, giving an indication of the oscillation build-up time of the OPO, highlighted by the grey area on the plot. The build-up times for the 500-ns window and the 25-ns window are 130 ns and 15 ns respectively. This

OSA CONTINUUM

shows that build-up time decreases for smaller time-windows due to the higher pump peak power. However, the build-up time to burst-pulse time-window ratio is much lower for 500-ns (130/500) compared to 25-ns (15/25), leading to less efficient conversion for the shorter window duration. Nevertheless, the burst-mode operation provided a compact OPO device offering flexible control of MIR pulse repetition-rate and peak-power. The burst-mode OPO also provided good power and pulse stabilities (beyond the short initial build up transient) similar to that during cw-pulsed operation, with those different time-window settings because of the oscillated signals all reached a steady state which generally suppress the pulse-to-pulse fluctuation [12]. In order to improve the conversion efficiency of the burst-mode OPO, shaping the pump burst-window profile could be considered. For example, pumping with 'figure-of-h' shaped pulses [18], where a higher intensity at the beginning of the window can reduce the build-up time followed by moderate intensities to avoid the back-conversion, would result in an increase of the overall conversion efficiency. Further investigations are underway.

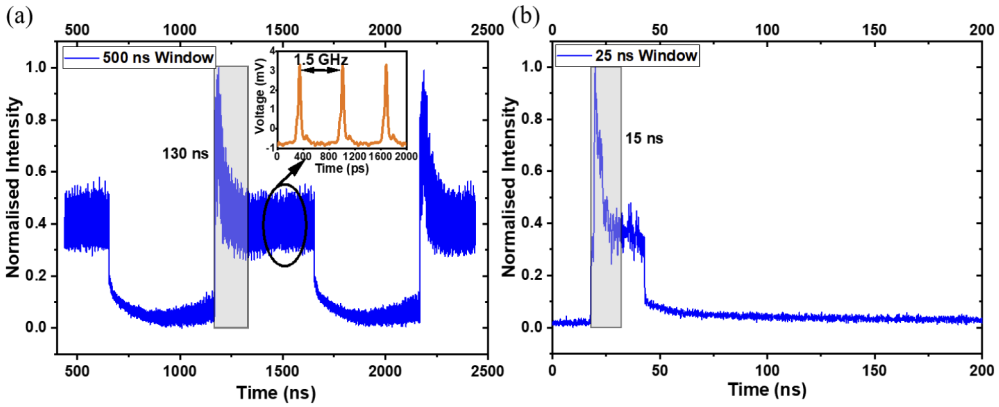

Fig. 8. Burst pulse traces of the residual pump (a) 500 ns and (b) 25 ns burst window times. The grey area highlights the cavity build-up time.

4. Conclusion

In conclusion, we present a widely tunable, high-repetition-rate, compact MIR picosecond PPLN OPO with controllable peak powers through burst-mode operation. A tunable idler wavelength range of 2260–3573 nm was realized. Under cw-pulsed operation at a 1.5-GHz repetition rate, a maximum idler average power of 2.4 W (~30 W peak power) was achieved for 14-W pump power. With the addition of an EOM to the MOPA to act as a time gate to suppress a variable number of pulses per 1 μs, burst-mode operation of the OPO at 1-MHz inter-burst repetition rate was demonstrated. Under burst mode operation, variable idler peak powers up to 1.2 kW were achieved. The oscillation build-up times for different pump burst-pulse time-windows and the consequent effect on conversion efficiency has also been studied. In the experiment, a minimum of 20-ns time-window was found to be sufficient to achieve an oscillation from the OPO and simultaneously provide high repetition rate and high peak power output.

Funding

Engineering and Physical Sciences Research Council (EP/P030181/1).

OSA CONTINUUM

Acknowledgments

The authors thank Prof. David Shepherd for helpful discussions during the manuscript preparation. The data from the figures can be found in DOI https://doi.org/10.5258/SOTON/D1524.

Disclosures

The authors declare no conflicts of interest.

References

1. M. W. Sigrist, "Mid-infrared laser-spectroscopic sensing of chemical species," J. Adv. Res. **6**(3), 529–533 (2015)..
2. R. Knappe, H. Haloui, A. Seifert, A. Weis, and A. Nebel, "Scaling ablation rates for picosecond lasers using burst micromachining," Laser-based Micro- and Nanopackaging and Assembly IV 7585, 75850H (2010).
3. Y. Su, W. Wang, X. Hu, H. Hu, X. Huang, Y. Wang, J. Si, X. Xie, B. Han, H. Feng, Q. Hao, G. Zhu, T. Duan, and W. Zhao, "10 Gbps DPSK transmission over free-space link in the mid-infrared," Opt. Express **26**(26), 34515–34528 (2018).
4. M. Mackanos, D. Simanovskii, K. Schriver, M. Hutson, C. Contag, J. Kozub, and E. Jansen, "Pulse-Duration-Dependent Mid-Infrared Laser Ablation for Biological Applications," IEEE J. Sel. Top. Quantum Electron. **18**(4), 1514–1522 (2012).
5. C. Gu, Z. Zuo, D. Luo, D. Peng, Y. Di, X. Zou, L. Yang, and W. Li, "High-repetition-rate femtosecond mid-infrared pulses generated by nonlinear optical modulation of continuous-wave QCLs and ICLs," Opt. Lett. **44**(23), 5848–5851 (2019).
6. A. Robertson, M. E. Klein, M. A. Tremont, K.-J. Boller, and R. Wallenstein, "2.5-GHz repetition-rate singly resonant optical parametric oscillator synchronously pumped by a mode-locked diode oscillator amplifier system," Opt. Lett. **25**(9), 657–659 (2000).
7. Q. Fu, L. Xu, S. Liang, P. C. Shardlow, D. P. Shardlow, S. Alam, and D. J. Richardson, "High-average-power picosecond mid-infrared OP-GaAs OPO," Opt. Express **28**(4), 5741–5748 (2020).
8. L. He, K. Liu, Y. Bo, Z. Liu, X. Wang, F. Yang, L. Yuan, Q. Peng, D. Cui, and Z. Xu, "30.5-μJ, 10-kHz, picosecond optical parametric oscillator pumped synchronously and intracavity by a regenerative amplifier," Opt. Lett. **43**(3), 539–542 (2018).
9. L. Xu, H.-Y. Chan, S.-U. Alam, D. J. Richardson, and D. P. Shepherd, "Fiber-laser-pumped, high-energy, mid-IR, picosecond optical parametric oscillator with a high-harmonic cavity," Opt. Lett. **40**(14), 3288–3291 (2015).
10. P. Jiang, C. Hu, T. Chen, P. Wu, B. Wu, R. Wen, and Y. Shen, "High Power Yb Fiber Laser With Picosecond Bursts and the Quasi-Synchronously Pumping for Efficient Midinfrared Laser Generation in Optical Parametric Oscillator," IEEE Photonics J. **8**(3), 1–7 (2016).
11. K. Wei, P. Jiang, B. Wu, T. Chen, and Y. Shen, "Fiber laser pumped burst-mode operated picosecond mid-infrared laser," Chin. Phys. B **24**(2), 024217 (2015).
12. K. Nagashima, Y. Ochi, and R. Itakura, "Optical parametric oscillator pumped by a 100-kHz burst-mode Yb-doped fiber laser," Opt. Lett. **45**(3), 674–677 (2020).
13. C. Kerse, H. Kalaycıoğlu, P. Elahi, B. Çetin, D. K. Kesim, Ö Akçaalan, S. Yavaş, M. D. Aşık, B. Öktem, H. Hoogland, R. Holzwarth, and FÖ Ilday, "Ablation-cooled material removal with ultrafast bursts of pulses," Nature **537**(7618), 84–88 (2016).
14. T. Liu, J. Wang J, G. I. Petrov, V. V. Yakovlev, and H. F. Zhang, "Photoacoustic generation by multiple picosecond pulse excitation," Med. Phys. **37**(4), 1518–1521 (2010).
15. H. H. P. Th Bekman, J. C. van den Heuvel, F. J. M. van Putten, and R. Schleijpen, "Development of a mid-infrared laser for study of infrared countermeasures techniques", Proc. SPIE 5615, Technologies for Optical Countermeasures, (2004).
16. L. Wang, T. Xing, S. Hu, X. Wu, H. Wu, J. Wang, and H. Jiang, "Mid-infrared ZGP-OPO with a high optical-to-optical conversion efficiency of 75.7%," Opt. Express **25**(4), 3373–3380 (2017).
17. S. Sharabi, G. Porat, and A. Arie, "Improved idler beam quality via simultaneous parametric oscillation and signal-to-idler conversion," Opt. Lett. **39**(7), 2152–2155 (2014).
18. S. Cai, M. Ruan, B. Wu, Y. Shen, and P. Jiang, "High Conversion Efficiency, Mid-Infrared Pulses Generated via Burst-Mode Fiber Laser Pumped Optical Parametric Oscillator," IEEE Access **8**, 64725–64729 (2020).
19. Z. Sacks, O. Gayer, E. Tal, and A. Arie, "Improving the efficiency of an optical parametric oscillator by tailoring the pump pulse shape," Opt. Express **18**(12), 12669–12674 (2010).